
Domain-Constrained Diffusion Models to Synthesize Tabular Data: A Case Study in Power Systems

Milad Hoseinpour¹ Vladimir Dvorkin¹

Abstract

Growing concerns over privacy, security, and legal barriers are driving the rising demand for synthetic data across domains such as healthcare, finance, and energy. While generative models offer a promising solution to overcome these barriers, their utility depends on the incorporation of domain-specific knowledge. We propose to synthesize data using a guided diffusion model that integrates domain constraints directly into the generative process. We develop the model in the context of power systems, with potential applicability to other domains that involve tabular data. Specifically, we synthesize statistically representative and high-fidelity power flow datasets. To satisfy domain constraints, e.g., Kirchhoff laws, we introduce a gradient-based guidance to steer the sampling trajectory in a feasible direction. Numerical results demonstrate the effectiveness of our approach.

1. Introduction

Synthetic data offers a viable solution for training machine learning (ML) models when real-world data is limited due to privacy and security concerns, legal barriers, etc. (Dahmen & Cook, 2019; Hoseinpour et al., 2023a; Lee & Hess, 2021). However, generating high-quality synthetic data requires more than merely replicating statistical patterns. To be useful, synthetic data should also conform to domain-specific constraints that reflect real-world feasibility (Li et al., 2025). This need underscores the importance of incorporating domain constraints into generative models. For instance, in healthcare, patient records must remain medically plausible (Gonzales et al., 2023); in finance, generated transactions

¹Department of Electrical and Computer Engineering, University of Michigan, Ann Arbor, USA. Correspondence to: Milad Hoseinpour <miladh@umich.edu>, Vladimir Dvorkin <dvorkin@umich.edu>.

must obey accounting principles (Zhang et al., 2020; Butler & Kwon, 2023); in chemistry and biology, synthetic molecules must satisfy structural and physical laws (van Breugel et al., 2024). In power systems, domain constraints are especially critical. Training ML models on data that violate fundamental physical laws such as Kirchhoff’s or Ohm’s laws can result in models that are more likely to produce infeasible or even unsafe decisions, leading to instability, blackouts, or equipment damage (Stiasny et al., 2022; Arteaga et al., 2019).

To support the development of trustworthy ML models for power systems, this paper focuses on generating high-quality synthetic power flow data that respect the domain constraints. One area where such data is particularly critical is the optimal power flow (OPF) problem. Indeed, the growing integration of renewable energy sources (RESs) has intensified the demand for faster and more scalable decision-making tools such as ML-based OPF solvers (Liu et al., 2022; Chatzos et al., 2021). However, training trustworthy ML-based OPF solvers relies heavily on large-scale and high-quality datasets. Yet, access to real-world power flow data is often limited due to privacy and security concerns (Joswig-Jones et al., 2022; Bugaje et al., 2023; Hoseinpour et al., 2023b; Wu & Dvorkin, 2025; Dvorkin & Botterud, 2023). This paper addresses this challenge by developing a domain-constrained diffusion model that learns the underlying distribution of historical power flow data and generates synthetic samples that are both statistically representative and feasible with respect to power flow constraints.

1.1. Related Work

In recent years, the application of advanced generative models such as variational autoencoders (VAEs), generative adversarial networks (GANs), and diffusion models has gained significant attention in power systems research for generating realistic synthetic data (Zhang et al., 2024). For instance, a VAE is developed in (Pan et al., 2019) to generate synthetic electric vehicles load profiles. In (Wang et al., 2022a), authors develop a representative multivariate load state generation mechanism based on conditional VAEs, where the goal is to synthesize snapshots of multi-area electricity demand. Authors in (Wang et al., 2022b) describe a conditional VAE

for synthesizing load profiles of industrial and commercial customers, which is conditioned on the month of the year and typical power exchange with the grid. However, VAEs may struggle with complex and high-dimensional datasets and result in low quality samples (Larsen et al., 2016). Moreover, there is no principled approach for VAEs to control the generated outputs, making it difficult to enforce domain-specific constraints during the generation process. GANs have also been used to synthesize load patterns in power systems (Zhang et al., 2018; Gu et al., 2019; Fekri et al., 2019). For instance, authors in (El Kababji & Srikantha, 2020) propose a GAN-based framework to generate synthetic appliance-level load patterns and usage habits. In (Chen et al., 2018), authors propose a GAN-based framework for renewable energy scenario generation that effectively captures both temporal and spatial patterns across a large number of correlated resources. Nonetheless, GANs also suffer from issues such as training instability, mode collapse, and similarly lack a principled approach for controllability (Jabbar et al., 2021).

Addressing the limitations of GANs and VAEs, diffusion models have emerged as the leading choice for generative models (Dhariwal & Nichol, 2021). A physics-informed diffusion model is proposed in (Zhang et al., 2024) for generating synthetic net load data, where the solar PV system performance model is embedded into the diffusion model. In (Dong et al., 2023), authors propose a conditional latent diffusion model for short-term wind power scenario generation, which uses weather predictions as conditional inputs. Authors in (Li et al., 2024) developed a framework based on diffusion models to generate electric vehicle charging demand time-series data, which is also capable of capturing temporal correlation between charging stations.

While these studies highlight the potential applications of diffusion models in power systems, they primarily focus on statistical consistency. To the best of our knowledge, no prior work has explored the integration of domain constraints such as the power flow equations directly into the diffusion process to ensure that the generated samples adhere to the operational laws governing power systems.

1.2. Contribution

We propose a generative modeling framework that leverages historical operational data from power systems to synthesize credible power flow datasets for ML research. The main contributions of this paper can be summarized as follows.

Synthesizing statistically representative power flow datasets: We develop a diffusion-based model capable of producing high-quality power flow datasets that matches the underlying statistical properties of real-world datasets. We synthesize active power injections \mathbf{p} , reactive power injections \mathbf{q} , voltages \mathbf{v} , and phase angles $\boldsymbol{\theta}$ across the network. How-

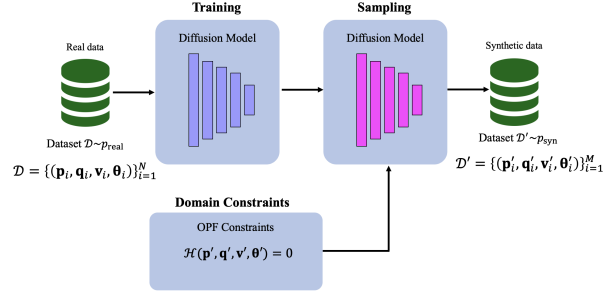


Figure 1. A high-level view of the problem setup.

ever, the model can be easily extended to synthesize other features, e.g., active power flow, reactive power flow.

Data fidelity with respect to the power flow constraints:

We introduce a guidance mechanism during the sampling phase of the diffusion model to ensure that the synthesized power flow data points are not only statistically representative but also feasible with respect to the power flow constraints. Specifically, we incorporate a constraint-aware guidance term at each denoising step. The guidance term corresponds to a single iteration of Riemannian gradient descent on the clean data manifold to minimize the data consistency loss. This gradient step pushes the evolving sample toward feasibility without altering the learned data distribution. Therefore, the synthesized power flow data points are not only feasible but also statistically representative.

2. Problem Setup

Consider a real dataset \mathcal{D} of power flow records $\{(\mathbf{p}_i, \mathbf{q}_i, \mathbf{v}_i, \boldsymbol{\theta}_i)\}_{i=1}^N$ of size N . Our goal is to generate a synthetic dataset $\mathcal{D}' = \{(\mathbf{p}'_i, \mathbf{q}'_i, \mathbf{v}'_i, \boldsymbol{\theta}'_i)\}_{i=1}^M$ of size M , which is both statistically representative of the given dataset \mathcal{D} and has high fidelity with respect to the power flow constraints. Thus, a synthetic dataset \mathcal{D}' should satisfy the following conditions:

$$\mathbf{dist}(p_{\text{syn}} || p_{\text{real}}) \leq \epsilon, \quad (1a)$$

$$\mathcal{H}(\mathbf{p}'_i, \mathbf{q}'_i, \mathbf{v}'_i, \boldsymbol{\theta}'_i) = 0, \quad \forall i = 1, \dots, M. \quad (1b)$$

where $\mathbf{dist}(\cdot || \cdot)$ is a distance measure between the real p_{real} and synthetic p_{syn} probability distributions, ϵ is a discrepancy threshold, and \mathcal{H} is the power flow constraints vector function.

Figure 1 gives a high-level view of the problem setup. We first train a diffusion model based on \mathcal{D} to learn the underlying probability distribution p_{real} . Then, we sample from the learned distribution p_{syn} to build a synthetic dataset \mathcal{D}' . To ensure the feasibility of the synthetic samples, we guide the sampling process using the power flow constraints.

3. Preliminaries

3.1. Diffusion Models

Diffusion models are generative models that synthesize new data points using two processes: forward and reverse. Consider $\mathbf{x}_0 = (\mathbf{p}, \mathbf{q}, \mathbf{v}, \boldsymbol{\theta})$ as a real power flow data point from the underlying distribution of the real data $p_{\text{real}} = q_0$. The forward process is a Markov chain that incrementally adds Gaussian noise to a real data point $\mathbf{x}_0 \sim q_0$ and transform it into pure noise through a fixed sequence of steps. For each time step $\{t\}_{t=1}^T$, the diffusion transition kernel is

$$q(\mathbf{x}_t | \mathbf{x}_{t-1}) = \mathcal{N}(\mathbf{x}_t; \sqrt{1 - \beta_t} \mathbf{x}_{t-1}, \beta_t \mathbf{I}), \quad (2)$$

where β_t is a small positive constant controlling the amount of noise added at each step (Ho et al., 2020). Due to (2), we can directly obtain \mathbf{x}_t from \mathbf{x}_0 by

$$\mathbf{x}_t = \sqrt{\bar{\alpha}_t} \mathbf{x}_0 + \sqrt{1 - \bar{\alpha}_t} \boldsymbol{\epsilon}, \quad (3)$$

where $\alpha_t = 1 - \beta_t$ and $\bar{\alpha}_t = \prod_{s=1}^t \alpha_s$.

The reverse process aims to recover the underlying data distribution q_0 from the tractable noise distribution q_T . It is modeled as a parameterized Markov chain:

$$p_\theta(\mathbf{x}_{t-1} | \mathbf{x}_t) = \mathcal{N}(\mathbf{x}_{t-1}; \mu_\theta(\mathbf{x}_t, t), \Sigma_\theta(\mathbf{x}_t, t)), \quad (4)$$

with the mean $\mu_\theta(\cdot, t)$ and covariance $\Sigma_\theta(\cdot, t)$ functions learned using neural networks parametrized by θ (Ho et al., 2020).

To train the neural networks in (4) and optimize the parameters θ so that the learned reverse process effectively inverts the forward diffusion, the loss function is simplified to a mean-squared error between the actual noise $\boldsymbol{\epsilon}$ added during the forward process and the noise $\boldsymbol{\epsilon}_\theta$ predicted by the neural network:

$$\mathcal{L}_{\text{diff}} = \mathbb{E}_{\mathbf{x}_0, \boldsymbol{\epsilon}, t} [\|\boldsymbol{\epsilon} - \boldsymbol{\epsilon}_\theta(\sqrt{\bar{\alpha}_t} \mathbf{x}_0 + \sqrt{1 - \bar{\alpha}_t} \boldsymbol{\epsilon}, t)\|^2], \quad (5)$$

where $\boldsymbol{\epsilon} \sim \mathcal{N}(0, \mathbf{I})$ and $\bar{\alpha}_t$ is defined as before. Algorithm 1 summarizes the implementation of the training process for (5) (Ho et al., 2020).

After training the model, new data points can be generated using the predicted clean sample $\hat{\mathbf{x}}_0$ at each step t via Tweedie's formula:

$$\hat{\mathbf{x}}_0(\mathbf{x}_t, t) = \frac{1}{\sqrt{\bar{\alpha}_t}} (\mathbf{x}_t - \sqrt{1 - \bar{\alpha}_t} \boldsymbol{\epsilon}_\theta(\mathbf{x}_t, t)), \quad (6)$$

and then

$$\mathbf{x}_{t-1} = \frac{\sqrt{\bar{\alpha}_t}(1 - \bar{\alpha}_{t-1})}{1 - \bar{\alpha}_t} \mathbf{x}_t + \frac{\sqrt{\bar{\alpha}_{t-1}}\beta_t}{1 - \bar{\alpha}_t} \hat{\mathbf{x}}_0 + \sigma_t \mathbf{z}, \quad (7)$$

where $\mathbf{z} \sim \mathcal{N}(0, \mathbf{I})$, $\sigma_t = \beta_t(1 - \bar{\alpha}_{t-1}) / (1 - \bar{\alpha}_t)$, and t starts from T to 1 (Song et al., 2020). Algorithm 2 summarizes the implementation of the sampling process (Ho et al., 2020).

Algorithm 1 : Training the diffusion model

Inputs: initialized neural network $\boldsymbol{\epsilon}_\theta$, noise schedule $\{\alpha_t\}_{t=1}^T$, dataset of \mathbf{x}_0 's sampled from q_0

Outputs: trained neural network $\boldsymbol{\epsilon}_\theta$

- 1: **repeat**
- 2: $\mathbf{x}_0 \sim q_0(\mathbf{x}_0)$
- 3: $t \sim \text{Uniform}(\{1, \dots, T\})$
- 4: $\boldsymbol{\epsilon} \sim \mathcal{N}(0, \mathbf{I})$
- 5: Take gradient descent step on

$$\nabla_\theta \|\boldsymbol{\epsilon} - \boldsymbol{\epsilon}_\theta(\sqrt{\bar{\alpha}_t} \mathbf{x}_0 + \sqrt{1 - \bar{\alpha}_t} \boldsymbol{\epsilon}, t)\|^2$$

- 6: **until** converged
-

Algorithm 2 : Sampling new data points

Inputs: trained neural network $\boldsymbol{\epsilon}_\theta$, noise schedule $\{\alpha_t\}_{t=1}^T$, noise scale σ_t

Outputs: new data point \mathbf{x}_0

- 1: $\mathbf{x}_T \sim \mathcal{N}(0, \mathbf{I})$
 - 2: **for** $t = T, \dots, 1$ **do**
 - 3: $\hat{\mathbf{x}}_0 \leftarrow \frac{1}{\sqrt{\bar{\alpha}_t}} (\mathbf{x}_t - \sqrt{1 - \bar{\alpha}_t} \boldsymbol{\epsilon}_\theta(\mathbf{x}_t, t))$
 - 4: $\mathbf{z} \sim \mathcal{N}(0, \mathbf{I})$ if $t > 1$, else $\mathbf{z} = 0$
 - 5: $\mathbf{x}_{t-1} \leftarrow \frac{\sqrt{\bar{\alpha}_t}(1 - \bar{\alpha}_{t-1})}{1 - \bar{\alpha}_t} \mathbf{x}_t + \frac{\sqrt{\bar{\alpha}_{t-1}}\beta_t}{1 - \bar{\alpha}_t} \hat{\mathbf{x}}_0 + \sigma_t \mathbf{z}$
 - 6: **end for**
 - 7: **return** \mathbf{x}_0
-

3.2. Power Flow Constraints

The schematic shown in Figure 2 illustrates the grid topology and notation used throughout this section. Let \mathcal{B} denote the set of buses and \mathcal{L} denote the set of transmission lines in a power grid. Moreover, let vectors \mathbf{p} and \mathbf{q} indexed as p_b and q_b denote the active and reactive power injections, respectively, at every bus $b \in \mathcal{B}$. Vectors \mathbf{v} and $\boldsymbol{\theta}$ indexed as v_b and θ_b stand for the voltage magnitudes and voltage angles, respectively, at every bus $b \in \mathcal{B}$. For compact representation, we omit shunt admittances in the formulation, though they are included in our numerical results.

For each bus $b \in \mathcal{B}$, power flow equality constraints can be

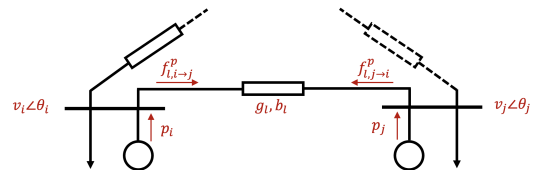


Figure 2. Schematic diagram of the power grid.

represented as

$$p_b - \sum_{l \in \mathcal{L}: i=b} f_{l,i \rightarrow j}^p - \sum_{l \in \mathcal{L}: j=b} f_{l,j \rightarrow i}^p = 0, \quad (8a)$$

$$q_b - \sum_{l \in \mathcal{L}: i=b} f_{l,i \rightarrow j}^q - \sum_{l \in \mathcal{L}: j=b} f_{l,j \rightarrow i}^q = 0, \quad (8b)$$

where Equation (8a) and (8b) enforce the active and reactive nodal power balance. The explicit expression for active power flows $f_{l,i \rightarrow j}^p$ and reactive power flows $f_{l,i \rightarrow j}^q$ on each transmission line $l \in \mathcal{L}$ from node i to node j are given by:

$$f_{l,i \rightarrow j}^p = v_i v_j [g_l \cos(\theta_i - \theta_j) + b_l \sin(\theta_i - \theta_j)] \quad (9a)$$

$$f_{l,i \rightarrow j}^q = v_i v_j [g_l \sin(\theta_i - \theta_j) - b_l \cos(\theta_i - \theta_j)], \quad (9b)$$

where $g_l = G_{ij}$ and $b_l = B_{ij}$ are the real and imaginary parts of the grid admittance matrix $Y = G + jB$. Note that due to line power losses, we have $f_{l,i \rightarrow j}^p \neq f_{l,j \rightarrow i}^p$ and $f_{l,i \rightarrow j}^q \neq f_{l,j \rightarrow i}^q$ (Molzahn et al., 2019).

4. Diffusion Guidance based on Power Flow Constraints

Theoretically, a diffusion model trained on a dataset of feasible power flow data points should satisfy the power flow constraints. But, in practice, it may generate data points that are infeasible due to learning and sampling errors (Feng et al., 2024; Daras et al., 2023). Enforcing these underlying constraints on the diffusion model improves its statistical accuracy and also makes it more reliable for synthesizing feasible power flow data points.

Figure 3 illustrates the geometry of sampling in a diffusion model. This geometry is characterized by a sequence of manifolds $\{\mathcal{M}_i\}_{i=0}^T$. At the bottom, there exists a clean data manifold $\mathcal{M} = \mathcal{M}_0$, surrounded by noisier manifolds according to the noise schedule, where the noisy data resides. Furthermore, let $\mathcal{H}(\mathbf{x}) = 0$ represent the power flow equality constraints in (8a)-(8b), where its intersection with the clean data manifold \mathcal{M} is the ideal sample \mathbf{x}_0^* . Accordingly, reverse diffusion steps can be characterized as mere transitions from manifold \mathcal{M}_i to \mathcal{M}_{i-1} . Due to Algorithm 2, the standard denoising process is oblivious to the domain constraints $\mathcal{H}(\mathbf{x}) = 0$. That is, no information about these constraints is incorporated into the sampling process.

To address this issue, we propose to incorporate a guidance term during the sampling process to encourage constraints satisfaction. The proposed guidance term inspired by manifold constrained gradients incorporates the required information (Chung et al., 2023). Specifically, we define a data consistency loss function based on the constraints $\mathcal{H}(\mathbf{x})$ residual:

$$R_{\mathcal{H}}(\mathbf{x}) = \|\mathcal{H}(\mathbf{x})\|_2^2, \quad (10)$$

and aim to minimize this loss over the clean data manifold \mathcal{M} , which is implicitly learned by the diffusion model:

$$\min_{\mathbf{x} \in \mathcal{M}} R_{\mathcal{H}}(\mathbf{x}). \quad (11)$$

To guide the sampling trajectory at each denoising step, we apply one step of Riemannian gradient descent with respect to (11):

$$\hat{\mathbf{x}}'_{0|t} = \hat{\mathbf{x}}_{0|t} - \tau_t \text{grad } R_{\mathcal{H}}(\hat{\mathbf{x}}_{0|t}), \quad (12)$$

where $\text{grad } R_{\mathcal{H}}(\hat{\mathbf{x}}_{0|t})$ denotes the Riemannian gradient of $R_{\mathcal{H}}$ at $\hat{\mathbf{x}}_{0|t}$, defined as the projection of the Euclidean gradient onto the tangent space of the manifold \mathcal{M} at $\hat{\mathbf{x}}_{0|t}$:

$$\text{grad } R_{\mathcal{H}}(\hat{\mathbf{x}}_{0|t}) = \mathcal{P}_{T_{\hat{\mathbf{x}}_{0|t}} \mathcal{M}} (\nabla_{\hat{\mathbf{x}}_{0|t}} R_{\mathcal{H}}(\hat{\mathbf{x}}_{0|t})). \quad (13)$$

Following the assumption of Chung et al. (Chung et al., 2022) that the clean data manifold \mathcal{M} can be locally approximated by an affine subspace, it can be proved that $\nabla_{\hat{\mathbf{x}}_{0|t}} R_{\mathcal{H}}(\hat{\mathbf{x}}_{0|t})$ is already tangential to the tangent space $T_{\hat{\mathbf{x}}_{0|t}} \mathcal{M}$:

$$\mathcal{P}_{T_{\hat{\mathbf{x}}_{0|t}} \mathcal{M}} (\nabla_{\hat{\mathbf{x}}_{0|t}} R_{\mathcal{H}}(\hat{\mathbf{x}}_{0|t})) \approx \nabla_{\hat{\mathbf{x}}_{0|t}} R_{\mathcal{H}}(\hat{\mathbf{x}}_{0|t}). \quad (14)$$

Substituting this approximation yields the following practical update rule for the guidance mechanism:

$$\hat{\mathbf{x}}'_{0|t} = \hat{\mathbf{x}}_{0|t} - \lambda_t \nabla_{\hat{\mathbf{x}}_{0|t}} R_{\mathcal{H}}(\hat{\mathbf{x}}_{0|t}), \quad (15)$$

where λ_t is a hyperparameter controlling the strength of the guidance at step t . The guidance term steers the sampling trajectory toward the intersection \mathbf{x}_0^* of the constraints $\mathcal{H}(\mathbf{x}) = 0$ and the clean data manifold \mathcal{M} , while preserving the generative distribution learned by the diffusion model. Due to Figure 3, at each step t , we have a 3-stage reverse diffusion step. First, we do a denoising step based on \mathbf{x}_t and estimate the clean data $\hat{\mathbf{x}}_{0|t}$. Second, we add the guidance term based on the gradient of the constraints residual function $R_{\mathcal{H}}(\hat{\mathbf{x}}_{0|t})$ and obtain $\hat{\mathbf{x}}'_{0|t}$. Third, by adding noise with respect to the corresponding noise schedule, we obtain \mathbf{x}_{t-1} . As previously discussed, the guidance term is tangential to the clean data manifold \mathcal{M} . Hence, $\hat{\mathbf{x}}'_{0|t}$ remains on the clean data manifold \mathcal{M} , which implies that the final sample is not only (approximately) feasible but also statistically representative. After constructing the gradient guidance term, it can be incorporated into the sampling process as shown in Algorithm 3. Due to step (4), the guidance term modifies the sampling path at each reverse diffusion step. We also omit the subscript t from the estimated clean data $\hat{\mathbf{x}}_{0|t}$ and denote it by $\hat{\mathbf{x}}_0$.

5. Numerical Results

In this section, we evaluate the performance of the proposed constrained diffusion model for synthesizing power flow datasets. We conduct experiments on the PJM 5-bus system

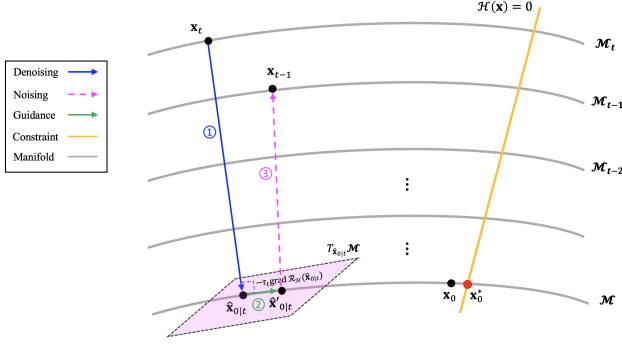


Figure 3. A schematic overview of the geometry of sampling with manifold constrained gradient guidance. At each step t , we have a 3-stage reverse diffusion step: (1) we do a denoising step based on \mathbf{x}_t and estimate the clean data $\hat{\mathbf{x}}_{0|t}$, (2) we add the guidance term based on the gradient of the constraints residual function $R_{\mathcal{H}}(\hat{\mathbf{x}}_{0|t})$ and obtain $\hat{\mathbf{x}}'_{0|t}$, and (3) by adding noise with respect to the corresponding noise schedule, we obtain \mathbf{x}_{t-1} .

(Babaeinejad et al., 2019). The effectiveness of our approach is assessed by comparing the statistical properties of the synthesized data against the real data and by analyzing the extent to which the power flow constraints are satisfied.

5.1. Experimental Setup

Since real-world power flow datasets are not publicly available, we synthetically generate the ground truth dataset by applying random perturbations around the nominal load $s_b^{\text{nom}} = (p_{d,b}^{\text{nom}}, q_{d,b}^{\text{nom}})$ at each bus $b \in \mathcal{B}$ of the system. Specifically, we uniformly sample active and reactive power demands at each bus $s_b = (p_{d,b}, q_{d,b}) \sim \mathcal{U}(0.8 s_b^{\text{nom}}, s_b^{\text{nom}})$. Given this new demand level, we solve a new instance of the corresponding AC-OPF problem and extract the feasible solutions $\mathbf{p}, \mathbf{q}, \mathbf{v}, \boldsymbol{\theta}$. Then, by stacking them together a single power flow data point $(\mathbf{p}_i, \mathbf{q}_i, \mathbf{v}_i, \boldsymbol{\theta}_i)$ is obtained for the ground truth dataset $\mathcal{D} = \{(\mathbf{p}_i, \mathbf{q}_i, \mathbf{v}_i, \boldsymbol{\theta}_i)\}_{i=1}^N$.

Algorithm 3: Sampling with gradient guidance

Inputs: trained neural network ϵ_θ , noise schedule $\{\alpha_t\}_{t=1}^T$, noise scale σ_t , guidance scale λ_t

Outputs: new data point \mathbf{x}_0

- 1: $\mathbf{x}_T \sim \mathcal{N}(0, \mathbf{I})$
 - 2: **for** $t = T - 1$ to 0 **do**
 - 3: $\hat{\mathbf{x}}_0 \leftarrow \frac{1}{\sqrt{\alpha_t}} (\mathbf{x}_t - \sqrt{1 - \alpha_t} \epsilon_\theta(\mathbf{x}_t, t))$
 - 4: $\hat{\mathbf{x}}'_0 \leftarrow \hat{\mathbf{x}}_0 - \lambda_t \nabla_{\hat{\mathbf{x}}_0} R_{\mathcal{H}}(\hat{\mathbf{x}}_0)$
 - 5: $\mathbf{z} \sim \mathcal{N}(0, \mathbf{I})$
 - 6: $\mathbf{x}_{t-1} \leftarrow \frac{\sqrt{\alpha_t(1-\alpha_{t-1})}}{1-\alpha_t} \mathbf{x}_t + \frac{\sqrt{\alpha_{t-1}\beta_t}}{1-\alpha_t} \hat{\mathbf{x}}'_0 + \sigma_t \mathbf{z}$
 - 7: **end for**
 - 8: **return** \mathbf{x}_0
-

Additional experimental details can be found in Appendix A.

5.2. Statistical Similarity

Figure 4 shows the histograms of power flow variables \mathbf{p} and \mathbf{q} for the real and synthetic datasets in the PJM 5-bus system. The histograms demonstrate that the synthesized power flow data points via the proposed model accurately captures the underlying statistical structure of the real data points. For instance, in sub-figure (a), the histograms of synthetic active power injections at Buses 2, 3, and 4 closely replicate the shape and spread characteristics of the real data. In sub-figure (b), the histograms of reactive power injections at Buses 1, 3, 4, and 5 exhibit multi-modal distributions. In each case, the synthetic data not only aligns well with the support of the real data but also successfully captures its prominent modes.

In addition to similarity of the marginal probability distributions, the proposed approach also ensures similarity of joint probability distributions. Figure 5 represents the real and synthetic joint probability distributions of active and reactive power injections at each bus of the system. The synthetic data points closely follow the distributional pattern of the real data. Moreover, in regions where the real data points are denser, the synthetic data points are also more concentrated, whereas in regions where the density of real data points decreases, the synthetic data points become more sparse. Another important property of the proposed approach is its coverage capability. As shown in Figure 5, the synthesized data points closely span the entire domain of the real joint probability distributions. Moreover, if the real data exhibit a multi-modal structure, the synthesized data points successfully capture all modes.

5.3. Constraint Satisfaction

To assess constraint satisfaction, we measure the magnitude of constraints violations for generated samples with and without the proposed guidance mechanism. Specifically, we focus on the active power balance constraint at each bus. Figure 6 presents histograms of the violation magnitudes for the active power balance constraints. As shown, without the guidance mechanism, a significant portion of the generated data points exhibit non-negligible violation for the active power balance constraints at Buses 1, 3, 4, and 5. In contrast, when the guidance mechanism is activated, the vast majority of generated samples show near-zero violation magnitudes at all buses, indicating strong satisfaction of the constraints.

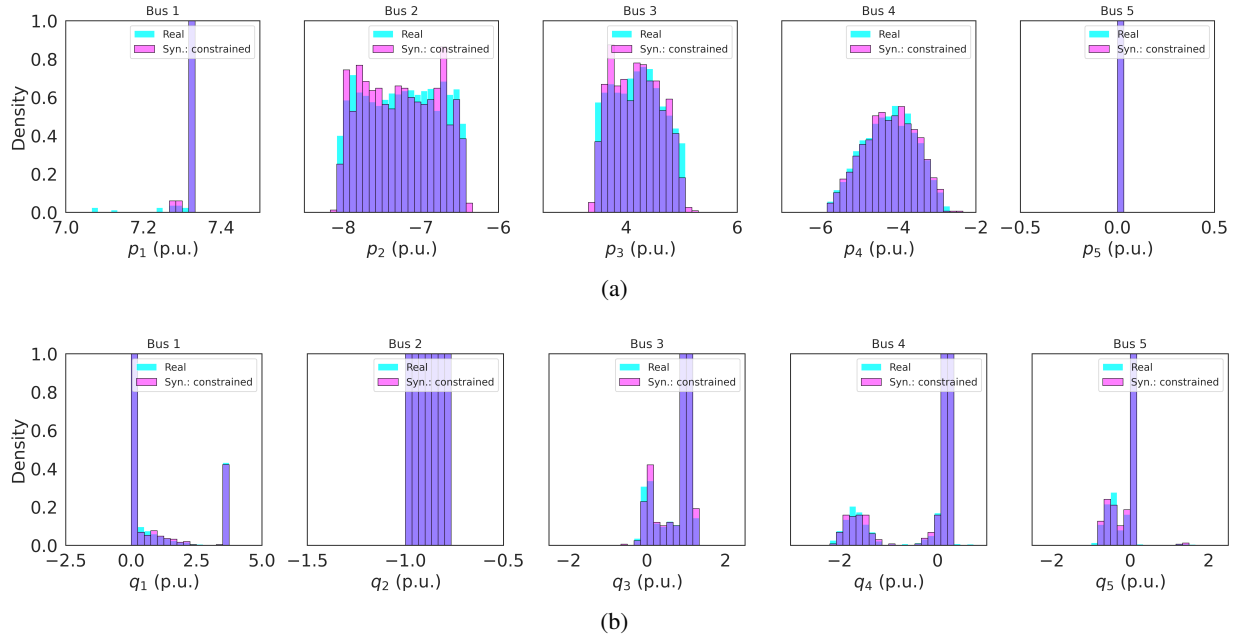


Figure 4. Histograms of the real versus synthetic (a) active and (b) reactive power injections at each bus of the system.

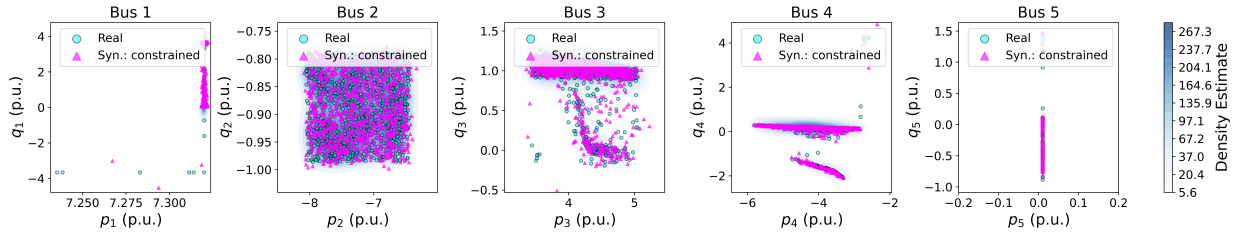


Figure 5. 2D scatter plots with density estimates of the active and reactive power injections at each bus, comparing the joint distributions of the real and constrained synthetic datasets. The plots highlight the ability of the diffusion model to replicate the underlying pattern, domain, and multi-modal structure of the real data.

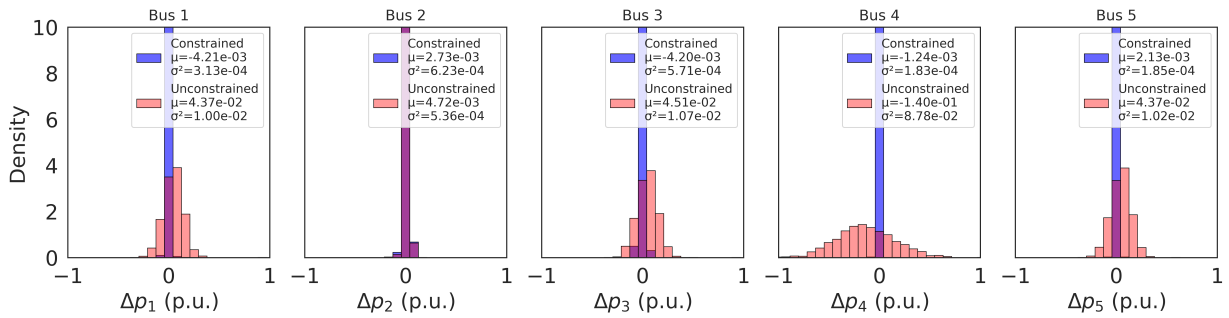


Figure 6. Histograms of violation magnitudes for the active power balance constraints, comparing synthesized data points from the guided and unguided diffusion models.

6. Conclusion

This paper presents a constrained diffusion model for generating synthetic tabular power flow data. Our results demonstrate that the generated data accurately replicate the marginal and joint distributions of the real power flow data. In particular, the model effectively captures all modes of the real data distribution and provides comprehensive coverage across its domain. Moreover, the proposed manifold-constrained gradient guidance enables the incorporation of domain constraints, specifically the physical laws of power systems, directly into the data generation process. This guidance steers the sampling trajectory toward feasibility, resulting in synthetic data that are not only statistically consistent but also physically meaningful.

Impact Statement

This paper presents work whose goal is to advance the field of Machine Learning. There are many potential societal consequences of our work, none which we feel must be specifically highlighted here.

References

- Arteaga, J.-M. H., Hancharou, F., Thams, F., and Chatzivasileiadis, S. Deep learning for power system security assessment. In *2019 IEEE Milan PowerTech*, pp. 1–6. IEEE, 2019.
- Babaeinejad, S., Birchfield, A., Christie, R. D., Coffrin, C., DeMarco, C., Diao, R., Ferris, M., Fliscounakis, S., Greene, S., Huang, R., et al. The power grid library for benchmarking ac optimal power flow algorithms. *arXiv preprint arXiv:1908.02788*, 2019.
- Bugaje, A.-A. B., Cremer, J. L., and Strbac, G. Generating quality datasets for real-time security assessment: Balancing historically relevant and rare feasible operating conditions. *International Journal of Electrical Power & Energy Systems*, 154:109427, 2023.
- Butler, A. and Kwon, R. H. Integrating prediction in mean-variance portfolio optimization. *Quantitative finance*, 23(3):429–452, 2023.
- Chatzos, M., Mak, T. W., and Van Hentenryck, P. Spatial network decomposition for fast and scalable ac-opf learning. *IEEE Transactions on Power Systems*, 37(4):2601–2612, 2021.
- Chen, Y., Wang, Y., Kirschen, D., and Zhang, B. Model-free renewable scenario generation using generative adversarial networks. *IEEE Transactions on Power Systems*, 33(3):3265–3275, 2018.
- Chung, H., Sim, B., Ryu, D., and Ye, J. C. Improving diffusion models for inverse problems using manifold constraints. *Advances in Neural Information Processing Systems*, 35:25683–25696, 2022.
- Chung, H., Lee, S., and Ye, J. C. Decomposed diffusion sampler for accelerating large-scale inverse problems. *arXiv preprint arXiv:2303.05754*, 2023.
- Dahmen, J. and Cook, D. Synsys: A synthetic data generation system for healthcare applications. *Sensors*, 19(5):1181, 2019.
- Daras, G., Dagan, Y., Dimakis, A., and Daskalakis, C. Consistent diffusion models: Mitigating sampling drift by learning to be consistent. *Advances in Neural Information Processing Systems*, 36:42038–42063, 2023.
- Dhariwal, P. and Nichol, A. Diffusion models beat gans on image synthesis. *Advances in neural information processing systems*, 34:8780–8794, 2021.
- Dong, X., Mao, Z., Sun, Y., and Xu, X. Short-term wind power scenario generation based on conditional latent diffusion models. *IEEE Transactions on Sustainable Energy*, 15(2):1074–1085, 2023.
- Dvorkin, V. and Botterud, A. Differentially private algorithms for synthetic power system datasets. *IEEE Control Systems Letters*, 7:2053–2058, 2023.
- El Kababji, S. and Srikantha, P. A data-driven approach for generating synthetic load patterns and usage habits. *IEEE Transactions on Smart Grid*, 11(6):4984–4995, 2020.
- Fekri, M. N., Ghosh, A. M., and Grolinger, K. Generating energy data for machine learning with recurrent generative adversarial networks. *Energies*, 13(1):130, 2019.
- Feng, B. T., Baptista, R., and Bouman, K. L. Neural approximate mirror maps for constrained diffusion models. *arXiv preprint arXiv:2406.12816*, 2024.
- Gonzales, A., Guruswamy, G., and Smith, S. R. Synthetic data in health care: A narrative review. *PLOS Digital Health*, 2(1):e0000082, 2023.
- Gu, Y., Chen, Q., Liu, K., Xie, L., and Kang, C. Gan-based model for residential load generation considering typical consumption patterns. In *2019 IEEE power & energy society innovative smart grid technologies conference (ISGT)*, pp. 1–5. IEEE, 2019.
- Ho, J., Jain, A., and Abbeel, P. Denoising diffusion probabilistic models. *Advances in neural information processing systems*, 33:6840–6851, 2020.

- Hoseinpour, M., Hoseinpour, M., and Aghagolzadeh, A. Accuracy improvement in differentially private logistic regression: A pre-training approach. *arXiv preprint arXiv:2307.13771*, 2023a.
- Hoseinpour, M., Hoseinpour, M., Haghifam, M., and Haghifam, M.-R. Privacy-preserving and approximately truthful local electricity markets: A differentially private vcg mechanism. *IEEE Transactions on Smart Grid*, 15(2):1991–2003, 2023b.
- Jabbar, A., Li, X., and Omar, B. A survey on generative adversarial networks: Variants, applications, and training. *ACM Computing Surveys (CSUR)*, 54(8):1–49, 2021.
- Joswig-Jones, T., Baker, K., and Zamzam, A. S. Opf-learn: An open-source framework for creating representative ac optimal power flow datasets. *2022 IEEE Power & Energy Society Innovative Smart Grid Technologies Conference (ISGT)*, pp. 1–5, 2022.
- Larsen, A. B. L., Sønderby, S. K., Larochelle, H., and Winther, O. Autoencoding beyond pixels using a learned similarity metric. In *International conference on machine learning*, pp. 1558–1566. PMLR, 2016.
- Lee, D. and Hess, D. J. Data privacy and residential smart meters: Comparative analysis and harmonization potential. *Utilities Policy*, 70:101188, 2021.
- Li, R., Sahu, D. R., Broeck, G. V. d., and Zeng, Z. Deep generative models with hard linear equality constraints. *arXiv preprint arXiv:2502.05416*, 2025.
- Li, S., Xiong, H., and Chen, Y. Diffcharge: Generating ev charging scenarios via a denoising diffusion model. *IEEE Transactions on Smart Grid*, 15(4):3936–3949, 2024.
- Liu, S., Wu, C., and Zhu, H. Topology-aware graph neural networks for learning feasible and adaptive ac-opf solutions. *IEEE Transactions on Power Systems*, 38(6):5660–5670, 2022.
- Molzahn, D. K., Hiskens, I. A., et al. A survey of relaxations and approximations of the power flow equations. *Foundations and Trends® in Electric Energy Systems*, 4(1-2):1–221, 2019.
- Pan, Z., Wang, J., Liao, W., Chen, H., Yuan, D., Zhu, W., Fang, X., and Zhu, Z. Data-driven ev load profiles generation using a variational auto-encoder. *Energies*, 12(5):849, 2019.
- Song, J., Meng, C., and Ermon, S. Denoising diffusion implicit models. *arXiv preprint arXiv:2010.02502*, 2020.
- Stiasny, J., Chevalier, S., Nellikkath, R., Sævarsson, B., and Chatzivasileiadis, S. Closing the loop: A framework for trustworthy machine learning in power systems. *arXiv preprint arXiv:2203.07505*, 2022.
- van Breugel, B., Liu, T., Oglic, D., and van der Schaar, M. Synthetic data in biomedicine via generative artificial intelligence. *Nature Reviews Bioengineering*, 2(12):991–1004, 2024.
- Wang, C., Sharifnia, E., Gao, Z., Tindemans, S. H., and Palensky, P. Generating multivariate load states using a conditional variational autoencoder. *Electric Power Systems Research*, 213:108603, 2022a.
- Wang, C., Tindemans, S. H., and Palensky, P. Generating contextual load profiles using a conditional variational autoencoder. In *2022 IEEE PES Innovative Smart Grid Technologies Conference Europe (ISGT-Europe)*, pp. 1–6. IEEE, October 2022b. doi: 10.1109/isgt-europe54678.2022.9960309. URL <http://dx.doi.org/10.1109/ISGT-Europe54678.2022.9960309>.
- Wu, S. and Dvorkin, V. Synthesizing grid data with cyber resilience and privacy guarantees. *arXiv preprint arXiv:2503.14877*, 2025.
- Zhang, C., Kuppannagari, S. R., Kannan, R., and Prasanna, V. K. Generative adversarial network for synthetic time series data generation in smart grids. In *2018 IEEE international conference on communications, control, and computing technologies for smart grids (SmartGridComm)*, pp. 1–6. IEEE, 2018.
- Zhang, S., Cheng, Y., and Yu, N. Generating synthetic net load data with physics-informed diffusion model. *arXiv preprint arXiv:2406.01913*, 2024.
- Zhang, Z., Zohren, S., and Roberts, S. Deep learning for portfolio optimization. *arXiv preprint arXiv:2005.13665*, 2020.

A. Additional Experimental Details

Noise Schedule. The forward diffusion process is defined using a linear noise schedule. Specifically, a sequence of noise levels $\{\beta_t\}_{t=1}^T$ is linearly spaced between 0.0001 and 0.02 over $T = 1000$ timesteps. These β_t values represent the variance of the added Gaussian noise at each step. From this schedule, the corresponding parameters $\{\alpha_t\}_{t=1}^T$, defined as $\alpha_t = 1 - \beta_t$, and the cumulative products $\{\bar{\alpha}_t\}_{t=1}^T$, with $\bar{\alpha}_t = \prod_{s=1}^t \alpha_s$, are computed and used to define the forward diffusion process in the model.

Denoyer Neural Network. The model employs a feedforward neural network, which is enhanced with sinusoidal time embeddings to capture temporal information. The architecture consists of an input layer projecting from the original feature space (20 dimensions) to the time embedding dimension (500). This is followed by a sinusoidal embedding layer to encode the timestep information. The network includes six hidden layers, each with 500 neurons, using ReLU activations, and concludes with an output layer that projects the result back to the original feature dimensionality (20).

Training Configuration. The model is trained on a dataset of 5000 samples using the Adam optimizer. The batch size is set to 500, and the model is trained for 15,000 epochs. The initial learning rate is set to 0.0001, with a learning rate schedule. The learning rate is decayed every 1500 steps by a factor of $\gamma = 0.6$.